Slow-light enhanced collinear second-harmonic generation in two-dimensional photonic crystals

Rumen Iliew,[1,*] Christoph Etrich,[2] Thomas Pertsch,[2] and Falk Lederer[1]
[1]*Institute of Condensed Matter Theory and Solid State Optics, Friedrich-Schiller-Universität Jena, Max-Wien-Platz 1, 07743 Jena, Germany*
[2]*Institute of Applied Physics/ultra optics, Friedrich-Schiller-Universität Jena, Max-Wien-Platz 1, 07743 Jena, Germany*
(Received 5 November 2007; revised manuscript received 14 January 2008; published 18 March 2008)

We predict an enhanced efficiency of collinear second-harmonic generation in photonic crystals. This can be achieved by taking advantage of the complexity of the dispersion relation in periodic lattices. Thus, two essential conditions for increasing the nonlinear interaction, namely, phase matching and small group velocity (slow light), can be met simultaneously. The analytical results based on a modal approach are verified with rigorous simulations by means of the finite-difference time-domain method. The influence of material dispersion on optimal phase match is discussed.

DOI: 10.1103/PhysRevB.77.115124 PACS number(s): 42.70.Qs, 42.65.Ky, 42.70.−a, 42.70.Mp

I. INTRODUCTION

In the early days of nonlinear optics, second-harmonic generation (SHG) was one of the first applications.[1] Since then, the quest for ever higher conversion efficiency is an ongoing challenge. Besides using materials with a larger nonlinear response, also, an exact control of the phase velocities of the interacting waves is crucial.[2] It was shown that for the optimal generation of the second harmonic (SH) from a strong fundamental harmonic (FH), the (possibly vectorial) phase matching condition $\mathbf{k}_1+\mathbf{k}_2=\mathbf{k}_3$ of the interacting plane waves has to be fulfilled, sometimes also called the momentum conservation condition. Here, $\mathbf{k}_1$ and $\mathbf{k}_2$ are the wave vectors of the two FHs and $\mathbf{k}_3$ is the wave vector of the generated SH. Because even in slightly anisotropic crystals the propagation direction, given by the direction of the group velocity, does not significantly differ from the direction of the phase velocity, the large interaction distances needed to obtain a large total conversion to the SH often require a copropagating scheme, where all three wave vectors involved are parallel. In addition, if diffraction is significant, it alters the mutual phase relations and the beam intensities and has to be adjusted to give optimum conversion.[3]

In the case of copropagating plane waves in homogeneous media, due to material dispersion, the phase matching condition is usually not fulfilled. However, the anisotropy of the common nonlinear crystals can be utilized to obtain phase matching between waves of different polarizations (ordinary and extraordinary) for certain angles of propagation. Then, the efficiency depends critically on maintaining this angle precisely (critical phase matching). Noncritical phase matching, where the deviation from the optimum angle only affects the condition at higher order, can be achieved for certain temperatures and propagation in the direction of the crystal's principal axes. However, for certain crystals, e.g., lithium niobate, the larger diagonal nonlinear coefficient can be used when quasi-phase-matching[1,2,4] is achieved by poling the nonlinear material with a certain periodicity, usually given by the so-called coherence length L_c which depends on the participating waves. With the recent interest in two-dimensional (2D) photonic crystals, also, quasi-phase-matching (QPM) with a 2D lattice of poled second-order nonlinear material[5,6] was achieved, leading to a much richer variety of phase matching conditions.

Earlier, the possibility of achieving phase matching using the more complex dispersion characteristics introduced by a one-dimensional (1D) periodic variation of linear properties of the dielectric structure was proposed[7–9] and experimentally verified.[10] Due to the recent interest in the field of photonic crystals, phase matching via a 1D periodic dielectric modulation regained scientific attention. In addition to providing phase matching, these structured materials also allow for a novel means of further increasing the conversion efficiency, relying on the small group velocity (and consequently the large density of states) near band edges[11–13] in finite 1D gratings and defects. In this model, the fields are propagated in time with one spatial transverse coordinate.

A decade ago, sum-frequency generation and phase matching in a 2D photonic crystal were investigated using a Green's function approach[14] in the undepleted-pump approximation (UDPA). Here, much more degrees of freedom (structure and propagation direction) for achieving phase matching exist. However, the approach presented cannot properly reproduce the results for a homogeneous medium in the UDPA and naturally fails if a substantial fraction of energy is converted to the SH field. A second application of 2D quadratically nonlinear photonic crystals (PhCs) was the utilization of a strong linear light localization at point defects within the band gap of the crystal, where generation of terahertz radiation,[15] SHG,[16] and optical parametric oscillators[17,18] were proposed theoretically.

Not long since, a 2D photonic crystal has been used to obtain phase matched (anti)collinear backward wave SHG, almost independent of the direction of propagation.[19] The calculations were carried out in the UDPA and a coherence length larger than 1200 μm was proposed. In demonstrating this, the problem was the length of the PhC which measured only 14 μm and thus should show reflections at the end facets. This Fabry-Pérot cavity with the resulting FH standing wave pattern of period 2 μm and the arbitrarily scaled fields make a distinction between the phase matched and nonphase-matched case very complicated. Another issue is the utilization of a higher (eighth) order band for the SH field which usually leads to large radiation losses in experimentally used PhC slab geometries. Recently, for weakly modu-

lated 2D PhCs, efficient parametric amplification of narrow beams has been proposed theoretically.[20] Here, the diffractionless regions of the dispersion relations of one wave could be used to get simultaneously phase matching for a large spectrum of transverse wave vectors and self-collimation of the generated beam. Due to the low index contrast and large period of the structure, the modeling could be performed by means of the paraxial wave equation.

Here, we investigate the usual collinear forward wave SHG in 2D PhCs, in principle, without further approximations (as mentioned above). Recently, the fabrication of 2D photonic crystals in $LiNbO_3$ was demonstrated.[21,22] Hence, we will focus on this material that is very common in integrated nonlinear optics and readily available as wafer in optical quality with exactly defined principal axes. We utilize the peculiar linear properties of light propagation in a properly designed 2D PhC to achieve noncritical collinear phase matching at a simultaneously low group velocity of the interacting waves to further enhance the SHG efficiency. We focus on wide beams neglecting transverse spatial effects, allowing for a description of the beams in terms of Bloch waves modified with an envelope that varies slowly in the propagation direction only.

In the following section, we derive equations for the slowly varying amplitudes of the underlying fast oscillating Bloch modes. Because we are interested in the power conversion efficiency rather than in the field amplitudes of the SHG, we use a physical scaling of the fields with respect to the power flux giving a nonlinear coefficient which directly allows to identify the influence of the interacting waves' group velocities. Apart from this effective nonlinearity, the efficiency will be shown also to depend strongly on the phase mismatch. In Sec. III, we introduce the 2D PhC structure and discuss the phase matching condition obtained from the linear properties of the crystal, where material dispersion is neglected. Because the crystal's anisotropy is of the same order as the material dispersion in the respective frequency range, it will be neglected as well at the first stage. We use a PhC with an air hole lattice of high index contrast; hence, light propagation cannot longer be modeled with the paraxial wave equation. Instead, in Sec. IV we present the results of the rigorous treatment of the nonlinear structure with the nonlinear finite-difference time-domain (FDTD) method.[23] We also identify a region in the PhC where backward wave SHG should be possible. In the next section, the influence of weak material dispersion and anisotropy is studied. Finally, we draw conclusions of the presented results.

II. ANALYTICAL APPROACH AND MODEL

By means of the Lorentz reciprocity theorem, we develop amplitude equations governing the propagation of light in a semi-infinite PhC half space without transverse spatial effects because we are mainly interested in the phase matching condition for wide beams without the influence of spatial walkoff or diffractive spreading. Instead, the individual interacting fields are described in terms of the normal modes of the linear crystal (the Bloch waves) with a slowly varying envelope in the propagation direction accounting for the nonlinear interaction and for dispersive effects due to the finite bandwidth.

As mentioned above, sum-frequency generation with Bloch waves in infinite photonic crystals was described in the UDPA using the Green's function method.[14] However, this approach cannot properly reproduce the results for a homogeneous medium in the same approximation. Recently, coupled equations of motion for slowly varying envelopes were obtained using a multiscale analysis starting from the wave equation for the electric field.[24] There, the electric field is expressed by means of Bloch waves at the respective frequencies of the three interacting waves with a time and position dependent slowly varying envelope. However, the influence of a phase mismatch was not considered.

Here, we focus on the efficiency of SHG for very wide beams with evolution in time and propagation direction. Starting from a given, possibly slowly time-dependent, field distribution in the plane $z=0$, we calculate the field evolution for propagation in the positive z direction. As in most modal approaches, we assume that the nonlinearity is small and, hence, the linear Bloch modes of the PhC are a good basis for this approach. These exact solutions of Maxwell's equations in the linear PhC are then modified by the perturbative polarization induced by the quadratic nonlinear interaction, leading to the evolution of the previously constant envelopes.

In the following analysis, we choose to work in regions of the dispersion relation of the PhC where only one band contributes to the propagation dynamics of the fundamental and second-harmonic wave. In this case, no concurrent three-wave mixing effects interfere with the SHG.

We use the conjugated form of the Lorentz reciprocity theorem[25] to obtain evolution equations for the envelopes. The theorem states that for two electromagnetic fields $(\mathbf{E}_1,\mathbf{H}_1)$ and $(\mathbf{E}_2,\mathbf{H}_2)$ inducing the respective dielectric polarizations $\mathbf{P}_1=\varepsilon_0\varepsilon_1(\mathbf{r},\omega)\mathbf{E}_1(\mathbf{r},\omega)$ and $\mathbf{P}_2=\varepsilon_0\varepsilon_1\mathbf{E}_2+\mathbf{P}_p(\mathbf{r},\omega)$ and satisfying Maxwell's equations, we have for nonabsorptive materials

$$\int_{\partial V} d\mathbf{A}\cdot[\mathbf{E}_1^*(\mathbf{r},\omega)\times\mathbf{H}_2-\mathbf{H}_1^*\times\mathbf{E}_2]=\imath\omega\int_V d^3\mathbf{r}\mathbf{P}_p\cdot\mathbf{E}_1^*, \tag{1}$$

where ∂V is the boundary of the (arbitrary) volume V. $\mathbf{P}_1$ is assumed to be linear to facilitate the exact solution of the (unperturbed) problem $(\varepsilon_1,\mathbf{E}_1,\mathbf{H}_1)$. For system 2, there is no perturbation of the linear properties, but we allow for a nonlinear perturbative polarization $\mathbf{P}_p$. In particular, we use the modal field of the Bloch waves of the fundamental and of the second harmonic,

$$\mathbf{E}_1(\mathbf{r},\omega)=\mathbf{e}^{f,s}_{n_{f,s}\mathbf{k}_{f,s}}(\mathbf{r})\exp[\imath k_{n_{f,s}z}(\omega)z], \tag{2}$$

$$\mathbf{H}_1(\mathbf{r},\omega)=\mathbf{h}^{f,s}_{n_{f,s}\mathbf{k}_{f,s}}(\mathbf{r})\exp[\imath k_{n_{f,s}z}(\omega)z], \tag{3}$$

where $\mathbf{e}^f_{n_f\mathbf{k}_f}$, $\mathbf{h}^f_{n_f\mathbf{k}_f}$, $\mathbf{e}^s_{n_s\mathbf{k}_s}$, and $\mathbf{h}^s_{n_s\mathbf{k}_s}$ denote the lattice-periodic electric and magnetic Bloch amplitudes of the fundamental (f) and second-harmonic (s) waves with corresponding Bloch vectors $\mathbf{k}_f=(0,0,k_{n_fz})$, $\mathbf{k}_s=(0,0,k_{n_sz})$ in the respective bands with indices n_f and n_s. As mentioned above, we as-

sume propagation in the z direction. Furthermore, only one Bloch mode should contribute to FH and SH. Usually, this is satisfied if the different bands are well separated in frequency or via different propagation directions. However, in certain cases, it may be necessary to include more modes in the analysis. The dispersion relation for perpendicular Bloch vectors $\omega=\omega_n(k_z)$ gives the relation between the Bloch vector and frequency for the subset $k_x=k_y=0$ of the three-dimensional $\mathbf{k}$ space. For practical reasons, we will use the inverted dispersion relation $k_z(\omega)$. Then, the Bloch amplitudes can be denoted by $\mathbf{e}_{f,s}(\mathbf{r},\omega)$, $\mathbf{h}_{f,s}(\mathbf{r},\omega)$ with an explicit frequency dependence. However, we restrict the bandwidth of the investigated processes to very narrow regions around ω_0 and $2\omega_0$ and, hence, assume that the frequency dependence of the Bloch amplitudes can be neglected, whereas we keep the dispersion of the Bloch vector.

Consequently, the *ansatz* for the perturbed problem $(\varepsilon_1,\mathbf{E}_2,\mathbf{H}_2,\mathbf{P}_p)$ in the time domain is

$$\begin{aligned}\begin{pmatrix}\mathbf{E}_2(\mathbf{r},t)\\ \mathbf{H}_2(\mathbf{r},t)\end{pmatrix} &= \frac{1}{2}a(z,t)\begin{pmatrix}\mathbf{e}_f(\mathbf{r},\omega_0)\\ \mathbf{h}_f(\mathbf{r},\omega_0)\end{pmatrix}\exp(\imath k_{fz}^0 z)\exp(-\imath\omega_0 t)\\ &+ \frac{1}{2}b(z,t)\begin{pmatrix}\mathbf{e}_s(\mathbf{r},2\omega_0)\\ \mathbf{h}_s(\mathbf{r},2\omega_0)\end{pmatrix}\exp(\imath k_{sz}^0 z)\exp(-2\imath\omega_0 t)\\ &+ (*),\end{aligned} \tag{4}$$

where $k_{fz}^0=k_{fz}(\omega_0)$ and $k_{sz}^0=k_{sz}(2\omega_0)$ are the central Bloch vectors and a and b the slowly varying envelopes of the fundamental and the second-harmonic waves, respectively. In the following, a periodicity of the structure in the z direction with period L is assumed. The volume V is chosen to be the respective unit cell Ω centered at the current z. This corresponds to a separation into a fast z dependence (fast oscillations on the scale of PhC period and Bloch amplitudes), which is integrated over, and a slow z dependence, which changes slowly over many periods and can be moved out of the integral. Inserting the Fourier transform of Eq. (4) into Eq. (1) and performing the integration along the boundaries in propagation direction, a difference equation for the amplitudes at next-nearest neighbor lattice sites is obtained.[26] For sufficiently small changes over one period L, these can be recast into differential equations. Using the rotating-wave approximation (RWA), we get for frequencies ω around ω_0,

$$\begin{aligned}\imath\frac{\partial\tilde{a}(z,\omega)}{\partial z} &+ [k_{fz}(\omega)-k_{fz}^0]\tilde{a}\\ &= -\frac{\omega}{2L\tilde{P}_f}\exp[\imath(k_{fz}(\omega)-k_{fz}^0)z]\int_{\Omega(z)}d^3\mathbf{r}'\mathbf{P}_p\cdot\mathbf{e}_f^*\\ &\quad\times\exp[-\imath k_{fz}(\omega)z'],\end{aligned} \tag{5}$$

and around $2\omega_0$,

$$\begin{aligned}\imath\frac{\partial\tilde{b}(z,\omega)}{\partial z} &+ [k_{sz}(\omega)-k_{sz}^0]\tilde{b}\\ &= -\frac{\omega}{2L\tilde{P}_s}\exp[\imath(k_{sz}(\omega)-k_{sz}^0)z]\int_{\Omega(z)}d^3\mathbf{r}'\mathbf{P}_p\cdot\mathbf{e}_s^*\\ &\quad\times\exp[-\imath k_{sz}(\omega)z'],\end{aligned} \tag{6}$$

where $\tilde{a}(z,\omega)$ is the Fourier transform of the slowly varying envelope $a(z,t)$. $\tilde{P}_{f,s}=0.5\,\mathrm{Re}\int dA(\mathbf{e}_{f,s}\times\mathbf{h}_{f,s}^*)_z$ is the modal power flux per unit cell in propagation direction for the unperturbed system and does not depend on z.[26] In order to utilize the (diagonal) major nonlinear coefficient d_{33} of $LiNbO_3$ which is five times larger than the minor coefficients, it is assumed that the electric fields of FH and SH are mainly polarized in the respective direction (Z) of the crystal system. Then, for the SHG process, we get from the total field [Eq. (4)] the following contribution to the nonlinear polarization:

$$\begin{aligned}\mathbf{P}_p(\mathbf{r},t) &= \frac{1}{2}[p_f(\mathbf{r},t)\exp(\imath k_{fz}^0 z-\imath\omega_0 t)+p_s\exp(\imath k_{sz}^0 z-2\imath\omega_0 t)]\mathbf{n}_x\\ &\quad+(*),\end{aligned} \tag{7}$$

where $\mathbf{n}_x$ is the unit vector denoting the polarization direction (x) of the electric field and, hence, of the nonlinear polarization ($Z\equiv x$) and p_f and p_s are the slowly (in t) varying envelopes of the polarization at ω_0 and $2\omega_0$, respectively. In the time domain, they are given by

$$p_f=2\varepsilon_0 d_{33}(-2\omega_0;\omega_0,\omega_0)ba^* e_{sx}(\mathbf{r})e_{fx}^*\exp[\imath(k_{sz}^0-2k_{fz}^0)z], \tag{8}$$

$$p_s=\varepsilon_0 d_{33}(-2\omega_0;\omega_0,\omega_0)a^2 e_{fx}^2\exp[\imath(2k_{fz}^0-k_{sz}^0)z]. \tag{9}$$

Due to the small difference $k_z(\omega)-k_z^0$, the exponentials in front of the integrals in Eqs. (5) and (6) can be moved into the integral. Expanding $k(\omega)$ by means of a Taylor series about the points ω_0 and $2\omega_0$, transforming back to the time domain, and using again the RWA, we obtain

$$\begin{aligned}\imath\frac{\partial a(z,t)}{\partial z}+\frac{\imath}{v_{gf}}\frac{\partial a}{\partial t}+ba^*\frac{\omega_0\varepsilon_0}{2L\tilde{P}_f}\int_{\Omega(z)}d^3\mathbf{r}'d_{33}(\mathbf{r}')\\ \times(e_{fx}^*)^2 e_{sx}\exp[\imath(k_{sz}^0-2k_{fz}^0)z']=0,\end{aligned} \tag{10}$$

$$\begin{aligned}\imath\frac{\partial b}{\partial z}+\frac{\imath}{v_{gs}}\frac{\partial b}{\partial t}+a^2\frac{\omega_0\varepsilon_0}{2L\tilde{P}_s}\int_{\Omega(z)}d^3\mathbf{r}'d_{33}(\mathbf{r}')e_{fx}^2 e_{sx}^*\exp[-\imath(k_{sz}^0\\ -2k_{fz}^0)z']=0,\end{aligned} \tag{11}$$

where $v_{gf}=c/n_{gf}=1/(\partial k_{fz}/\partial\omega)_{\omega_0}$ is the group velocity (GV) in the z direction. Here, we allow also for backward SHG, i.e., allow for a negative sign $\sigma=\mathrm{sgn}(v_{gs})$ of the SH GV, where consequently[27] also $\mathrm{sgn}(\tilde{P}_s)=\sigma$. We are interested in efficient nonlinear interaction. Hence, the oscillations of the exponentials in the integrals over z' should have a period larger than L. This is fulfilled if there exists one reciprocal lattice vector G_0 such that $\Delta k=k_{sz}^0-2k_{fz}^0+G_0$ is small, i.e., if $|\Delta k|\ll 2\pi/L$. This slowly varying exponential can be moved in front of the integral giving

$$\imath\frac{\partial a}{\partial z}+\frac{\imath}{v_{gf}}\frac{\partial a}{\partial t}+ba^*\exp(\imath\Delta kz)\frac{\omega_0\varepsilon_0\kappa}{2L\tilde{P}_f}=0, \tag{12}$$

$$\iota\frac{\partial b}{\partial z}+\frac{\iota}{v_{gs}}\frac{\partial b}{\partial t}+a^2\exp(-\iota\Delta kz)\frac{\omega_0\varepsilon_0\kappa^*}{2L\tilde{P}_s}=0, \tag{13}$$

with the nonlinear coefficient $\kappa=\int_\Omega d^3\mathbf{r}d_{33}(\mathbf{r})(e_{fx}^*)^2e_{sx}\times\exp(-\iota G_0 z)$. Utilizing the equivalence of energy and group velocity[27] and normalizing the fields with respect to their respective powers via $a=(P_0/\tilde{P}_f)^{0.5}A$, $b=(P_0/|\tilde{P}_s|)^{0.5}\times\exp(-\iota\varphi_0)B$, where P_0 is an arbitrary fixed normalization power and φ_0 the phase of κ [i.e., $\kappa=|\kappa|\exp(\iota\varphi_0)$], we obtain

$$\iota\frac{\partial A}{\partial z}+\frac{\iota}{v_{gf}}\frac{\partial A}{\partial t}+\gamma BA^*\exp(\iota\Delta kz)=0, \tag{14}$$

$$\iota\sigma\frac{\partial B}{\partial z}+\frac{\iota}{|v_{gs}|}\frac{\partial B}{\partial t}+\gamma A^2\exp(-\iota\Delta kz)=0, \tag{15}$$

with $\gamma=(2P_0/\varepsilon_0 c)^{0.5}\omega_0|d_{33}|/c\sqrt{A_{\text{eff}}}$. The effective area is defined by

$$A_{\text{eff}}=\frac{1}{n_{gf}^2}\frac{1}{|n_{gs}|}\frac{1}{L}\frac{\left(\int_\Omega d^3\mathbf{r}\varepsilon_f|\mathbf{e}_f|^2\right)^2\int_\Omega d^3\mathbf{r}\varepsilon_s|\mathbf{e}_s|^2}{\left|\int_{\Omega_{\text{nl}}}d^3\mathbf{r}(e_{fx}^*)^2e_{sx}\exp(-\iota G_0 z)\right|^2}, \tag{16}$$

where we have assumed that the nonlinearity is constant in $\Omega_{\text{nl}}\subset\Omega$ but vanishes elsewhere. Equations (12) and (13) are the well-known equations describing SHG with plane waves in a homogeneous medium.[2] In our physical power scaling of the equations, we obtain for the transported powers per transverse unit cell $P_{f(z)}=P_0|A(z)|^2$ and $P_{s(z)}=P_0|B(z)|^2$ for FH and SH, respectively.

For fixed powers (passing the cross section area $A_\perp=\Omega/L$ of the unit cell) of the two interacting fields, the strength of the nonlinearity is determined by A_{eff}. For a homogeneous medium, the effective area is just the area $A_\perp$ of the (virtual) unit cell multiplied with $\varepsilon_f^2\varepsilon_s/n_{gf}^2n_{gs}\approx n_f^2n_s$, i.e., it is determined by the refractive index of the medium at the two frequencies. However, in a structured periodic medium, the effective area can be reduced in two ways. First, the group indices can be much larger than the occurring refractive indices, e.g., for standing-wave-like fields close to certain high-symmetry points. This dependence of the nonlinear term on the group indices is in agreement with a different approach for coupled resonator optical waveguides.[28] Second, the fields can be concentrated much more in the nonlinear regions reducing the fraction with the field integrals in Eq. (16).

For the stationary, forward ($\sigma=1$) phase matched ($\Delta k=0$) case without SH input and with $A(0)=A_0$, we get the solution[2] $A(z)=A_0\,\text{sech}(\gamma|A_0|z)$, $B(z)=\iota A_0^2\tanh(\gamma|A_0|z)/|A_0|$. For a fundamental power input $P_0=P_f(0)$, we obtain for the actual powers per unit cell $P_f(z)=P_0\,\text{sech}^2(\gamma z)$, $P_s(z)=P_0\tanh^2(\gamma z)$, where it should be kept in mind that $\gamma\propto\sqrt{P_0}$.

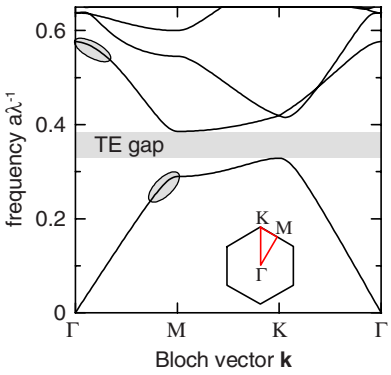

FIG. 1. (Color online) TE band structure diagram for the PhC with $r/a=0.3$ and $n=2.1588$. The gray ellipses mark the regions used for phase matching.

III. SLOW-LIGHT ENHANCED SECOND HARMONIC GENERATION

Most experimental investigations of 2D PhCs are performed in PhC slabs, where the slab waveguide provides vertical guidance of the light. Because the field dynamics is essentially in plane, here, we restrict to a truly two-dimensional photonic crystal, where y is the invariant direction of the system perpendicular to the plane of periodicity. We use a hexagonal lattice of air holes with hole radius r and lattice pitch a. First, we neglect the anisotropy and the material dispersion of $LiNbO_3$. Their influence will be considered later. We choose a refractive index of $n=2.1588$ corresponding to the extraordinary index at $\lambda=1$ μm and room temperature.[29] A ratio $r/a=0.3$ is used and the dispersion relation of the PhC is calculated solving Maxwell's equations with periodic boundary conditions by preconditioned conjugate-gradient minimization of the block Rayleigh quotient in a plane wave basis, using a freely available software package.[30] Introducing the normalized frequency $u=\omega a/2\pi c=a/\lambda$, a TE photonic band gap for $0.329<u<0.386$ is obtained. For a nonabsorbing photonic crystal, it can be shown that for a Bloch vector $\mathbf{k}_0$ where $2\mathbf{k}_0$ is a reciprocal lattice vector, $\omega_n(\mathbf{k}_0-\mathbf{k})=\omega_n(\mathbf{k}_0+\mathbf{k})$, i.e., the dispersion relation has an inversion symmetry center at $\mathbf{k}_0$. Hence, either the group velocity $\nabla_{\mathbf{k}}\omega_n(\mathbf{k})$ vanishes or the dispersion relation is degenerate at $\mathbf{k}_0$ or $\omega(\mathbf{k}_0)=0$. In the hexagonal crystal, the M point is such a high-symmetry point. Therefore, when the wave vector at the first band approaches M, the group velocity approaches 0. Obviously, the dispersion relation is also inversion symmetric with respect to Γ and, hence, also the GV of a nondegenerate band with $\omega(\Gamma)\neq 0$ vanishes at Γ. Combining these two slow light waves, the efficiency of the SHG process can be increased in two ways. From the band structure diagram shown in Fig. 1, it can be seen that the two marked regions correspond roughly to frequency regions separated by a factor of 2. Second, for $G_0=2M$ (which is equivalent to the Γ point in the neighboring Brillouin zone), a small Δk is obtained if k_{fz} is close to M and k_{sz} is negative and close to Γ. Then, both corresponding Bloch waves have a reduced positive GV, which should allow for efficient (forward) SHG.

For perfect phase matching $\Delta k=0$, in the extended zone scheme where $\mathbf{k}$ is not restricted to the first Brillouin zone,

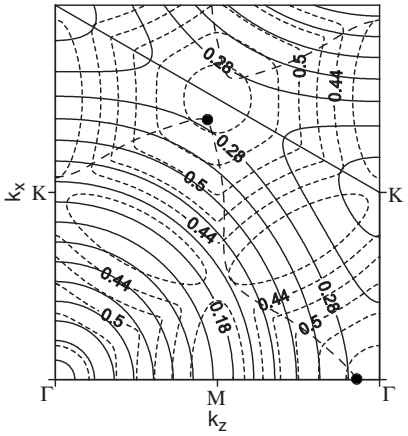

FIG. 2. Isofrequency curves for the PhC in Fig. 1. Band 1 (solid curves) is scaled by a factor of 2 [i.e., $\omega_1(\mathbf{k}/2)$]; the short-dashed curves correspond to (the unscaled) band 2. The long-dashed curve represents perfect phase match for collinear propagation; the black dots mark the points of collinear phase matching in the ΓM direction at $u=0.283\,53, 0.567\,06$.

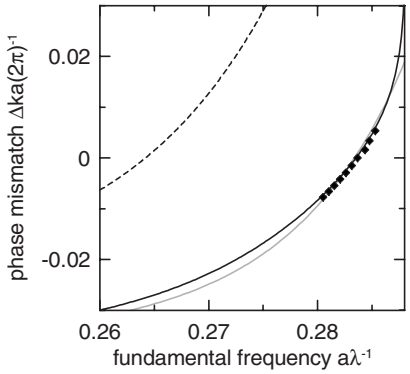

FIG. 3. Frequency dependence of the phase mismatch for collinear propagation in the ΓM direction and for $a=600$ nm. The solid black and the dashed curves denote the isotropic case without material dispersion and the anisotropic case with material dispersion, respectively, both for $r=180$ nm. The gray curve is the case with anisotropy and material dispersion with an increased hole radius of $r=195$ nm. The symbols are the results obtained from the nonlinear FDTD calculations for the isotropic case without material dispersion and for $r=180$ nm.

we can set $G_0=0$ and find $2\omega_{n_f}(\mathbf{k}_s/2)=\omega_{n_s}(\mathbf{k}_s)$ as the phase matching condition. The frequencies $\omega_{n_f}(\mathbf{k}/2)$ and $\omega_{n_s}(\mathbf{k}/2)$ are visualized in Fig. 2 by means of isofrequency lines in the 2D $\mathbf{k}$ space. The curve of the collinear phase match, given by the equation $\omega_{n_s}(\mathbf{k})-2\omega_{n_f}(\mathbf{k}/2)=0$, is superimposed on this graph, yielding the frequencies and Bloch vectors of phase match for arbitrary propagation directions. The points of exact phase matching in the ΓM direction are marked. From the dispersion relation, we obtain a fundamental frequency $u_0=0.283\,53$ with $k_{fz}^0=0.534\times 2\pi/a$ and the group indices $n_{gf}=3.8$ and $n_{gs}=5.2$. Because these points of phase match lie on a high symmetry line (ΓM), the respective isofrequency curves touch tangentially for phase matching. Thus, it is noncritical. In contrast, in other (nonsymmetrical) directions, the isofrequency curves intersect, giving already first-order contributions to Δk for small angular deviations of the pump beam from the exact angle of phase match resulting in critical phase matching. Moreover, in such nonsymmetrical directions, the directions of the group velocities of FH and SH differ significantly, leading to a strong spatial walkoff.

However, in the second high-symmetry direction ΓK, noncritical phase matching for backward SHG is achieved at a fundamental frequency $u_0=0.205$ for $n_{gf}=1.8$ because here the group index $n_{gs}=-15$ of the SH wave is negative ($\sigma=-1$). However, the modal overlap gives a much smaller efficiency. This process will be investigated in detail elsewhere.

Obviously, the presented hexagonal lattice allows for phase matched collinear forward SHG and backward SHG in the very same structure but for different propagation directions and frequencies. The dependence of the normalized phase mismatch on the normalized frequency u for collinear propagation in the ΓM direction is shown in Fig. 3.

Apart from phase matching and low group velocity, also, an efficient nonlinear coupling of the modal fields, i.e., a small effective area, is important. The important transverse field component E_x of FH and SH is depicted in Fig. 4. For the FH wave, the plane-wave-like behavior in the propagation (z) direction with a weak modulation in the transverse (x) direction can be clearly seen. A closer inspection of real and imaginary parts reveals the weakly standing-wave-like nature of the field in the z direction. The SH field has approximately half the period in the propagation direction and a much stronger transverse modulation due to a stronger interaction with the modulated dielectric, which effectively decreases the group velocity and, hence, enhances the nonlinear interaction.

From the integral of the modal fields, we obtain an effective area (in a 2D system an effective length) $A_{\text{eff}}=5.9a$, whereas for the homogeneous medium, we get $A_{\text{eff}}=10a$, corresponding to an enhancement of the nonlinear coefficient γ by a factor of 1.3. In the phase matched case, this translates into a scaling of the propagation distance, i.e., a faster growth of the SH intensity. The enhancement can be significantly increased by further reducing the group velocities while simultaneously maintaining phase matching. However, because for a given crystal geometry the only free parameter is the FH wavelength, the group velocity and the phase matching condition cannot be varied independently. Rather, a new degree of freedom has to be included, e.g., the ratio r/a. Then, due to the changes in the dispersion relation, the point of exact phase match in a fixed propagation direction will move, leading to a modified effective area. A favorable point

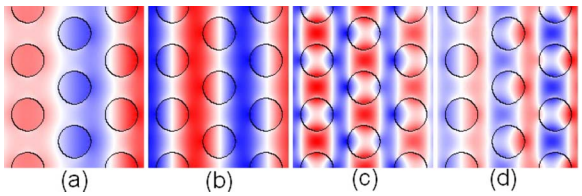

FIG. 4. (Color online) Spatial distribution of (a) real and (b) imaginary parts of e_{fx} and (c) real and (d) imaginary parts of e_{sx} for propagation from left to right.

would be approaching simultaneously the M and Γ points of the FH and SH waves at phase match which can be achieved if $\omega_2(\Gamma)=2\omega_1(M)$, corresponding to $r/a=0.32$. Thus, a maximum efficiency can be achieved for r/a slightly below this value at a FH frequency u slightly below 0.296. In the following section, we will investigate the efficiencies for the three values of r/a of 0.3, 0.31, and 0.315.

IV. RIGOROUS TREATMENT USING THE NONLINEAR FINITE-DIFFERENCE TIME-DOMAIN METHOD

Advances in computer hardware enabled the direct numerical treatment of microsized photonic components. We choose to model the system using the FDTD method,[23] where Maxwell's equations are discretized in time and space without further approximation. This treatment ensures that all effects of light propagation, e.g., field discontinuity at high-contrast dielectric interfaces, are properly accounted for. Moreover, the limits of frequently used approximations, e.g., the low-depletion limit,[19] can be identified. The quadratically nonlinear polarization of $LiNbO_3$ in the time domain used here [cf. Eqs. (8) and (9)] is given by

$$\mathbf{P}_{\mathrm{nl}}(\mathbf{r},t) = 2\varepsilon_0 d_{33}(-2\omega_0,\omega_0,\omega_0)E_x^2(\mathbf{r},t)\mathbf{n}_x, \qquad (17)$$

where E_x is the (real) x component of the electric field in the time domain. This means that the nonlinear response of the exciting electric field is instantaneous. Only the tensor component d_{33} (oriented along x in the laboratory frame) is taken into account and the others are neglected. For reasons of numerical stability, the nonlinear term is treated implicitly in the usually explicit FDTD scheme. However, due to the simpler form of Eq. (17), we solve the nonlinear equations analytically instead of using an iterative algorithm.[31]

Obviously, the investigation of phase matching effects in SHG requires an accurate numerical resolution of the phases of the fields. Special attention must be paid to the spatial discretization in the FDTD method in order to reduce phase mismatch[32] induced by the numerical dispersion to values which do not distort the results. From careful examinations of SHG in a homogeneous medium, we found a spatial discretization of $\Delta x=\lambda/424$ to be sufficient for the investigated propagation lengths. The time step was taken to be $\Delta t=\Delta x/2c$, relatively close to the (Courant) criterion[23] for numerical stability in order to introduce not too much additional numerical dispersion.

To reduce the numerical efforts, periodic boundary conditions in the direction perpendicular to the propagation direction ΓM were used. Hence, the spatial window consists of many conventional elementary cells (size $\sqrt{3}a\times a$) arranged along ΓM, with transverse period a. In the propagation direction, the computing window was terminated by perfectly matched layer boundaries.[23] As excitation, a plane wave of adjustable intensity and frequency was used at one end, in a short unstructured region before the PhC facet, thus approximating wide beams by Bloch waves. After a steady state was reached, discrete Fourier transforms at the FH and SH frequencies were applied to the fields at every grid point, leading to the corresponding (complex) fields in the Fourier domain. From this, all interesting quantities, as the Poynting vector or flux along the propagation direction, can be obtained. To obtain the time averaged power flux of FH and SH waves, we integrate the real part of the z component of the complex Poynting vector over the cross section (along x) at every z. To be able to compare the efficiencies for different frequency detunings, the input power at the very beginning of the PhC was kept constant for all calculations. A constant sum of FH and SH powers along the propagation direction confirms energy conservation and that almost no energy is transferred to other harmonics.

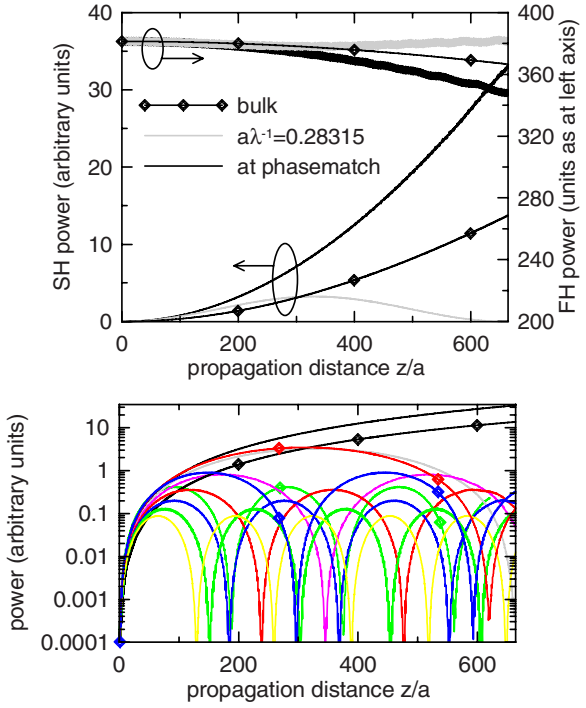

FIG. 5. (Color online) FH and SH power flux per transverse unit cell for selected pump frequencies on a linear scale (top) and SH power flux per transverse unit cell for all investigated pump frequencies (bottom). The same units were used for all power values. Black line: $u=0.283\,69$. The colored lines without diamonds correspond in order of decreasing oscillation period to the following pump frequencies: $u=0.283\,15, 0.282\,62, 0.282\,09, 0.281\,56, 0.281\,03, 0.280\,50$. The colored lines with diamond symbols correspond in the same order to $u=0.284\,36, 0.284\,77, 0.285\,31$. The black line with diamond symbols is for phase matched SHG in a (nondispersive) homogeneous medium with $u=0.283\,69$.

For different frequencies, the dependence of the FH and SH powers per transverse unit cell (here a) on z obtained from the FDTD calculations for $r/a=0.3$ is shown in Fig. 5. A periodically oscillating behavior can clearly be seen, except for $u=0.283\,69$ and for the case of a nondispersive, isotropic homogeneous medium, where the interaction is phase matched automatically. For frequency detunings from phase match to either side, it can be observed that the longer the periods, the higher the power at the SH maxima, in full accordance with the solutions[2] to Eqs. (14) and (15) for decreasing magnitude of the phase mismatch $|\Delta k|$. In the UDPA (e.g., for large phase mismatch: $|\Delta k| \gg 2\gamma$), we have $P_s(z)=P_0(2\gamma/\Delta k)^2 \sin^2(\Delta k z/2)$. This period is just twice the coherence length $L_c=\pi/|\Delta k|$, which easily allows us to obtain

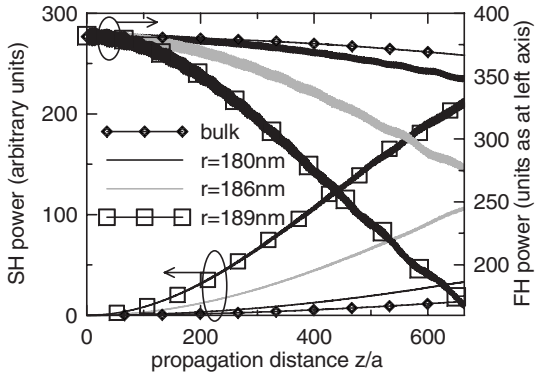

FIG. 6. Power per transverse unit cell along propagation for SHG obtained from FDTD calculations for different hole sizes and for pumping at the respective phase match wavelength (λ_f =2.115 μm for r=180 nm, λ_f=2.066 μm for r=186 nm, and λ_f =2.0455 μm for r=189 nm. Also, the case for a (nondispersive) homogeneous medium (bulk) with λ_f=2.115 μm is shown.

the absolute value of the phase mismatch reversely. However, comparing the cases u=0.284 77 and u=0.282 62 (see Fig. 5) in the first case of the slightly smaller period, the maximum conversion is still considerably higher. This is due to the generally lower group velocities for positive frequency detuning, leading to a larger effective nonlinearity. This is in full accordance with the modal equations because in the UDPA, the conversion period is not altered, but the maximum power depends on γ.

We calculated $|\triangle k|=2\pi/(z_1-z_0)$, where z_0 and z_1 are consecutive zeros of the SH power, and adjusted the sign manually. The results shown in Fig. 3 are in excellent agreement with the phase mismatch obtained from the linear calculations.

To investigate a further efficiency enhancement, we modeled also the cases of hole radii of 186 nm (r/a=0.31) and 189 nm (r/a=0.315), where both the FH and SH waves are even slower. As expected, we obtain even larger enhancements for a growing hole size (see Fig. 6).

To quantify the efficiency enhancements, we compare the SHG efficiency $\eta=P_s(L)/P_f^2(0)L^2$ for a small enough propagation length L to satisfy the UDPA, where $\tanh^2(x)\approx x^2$. Then, η is a geometry and material dependent constant. For the phase matched case, we obtain $\eta=(2/\varepsilon_0 c^3 A_{\text{eff}})(\omega_0|d_{33}|)^2$, and for the (unlikely) dispersionless homogeneous medium, the larger effective area discussed earlier has to be used here. For QPM in a homogeneous medium, this efficiency is further reduced by a factor $(2/\pi)^2$=41% (with the respective larger effective area).

From the parabolic behavior of the SH curves from the FDTD, we obtain an increase of η of the phase matched PhC with r=180 nm of 2.3 compared to the dispersionless homogeneous material, corresponding to a 5.7-fold increase compared to the more realistic QPM case. For the larger holes, we obtain an increase of 20 for r=186 nm and of 60 for r =189 nm compared to the QPM case.

V. INFLUENCE OF MATERIAL DISPERSION AND ANISOTROPY

For wide-beam SHG in homogeneous media, the phase mismatch is caused by the material dispersion and, depending on the polarizations, by the material anisotropy alone. Due to the usually resulting short coherence lengths, its control is vital for efficient conversion. However, in structured dielectrics, as layered systems, waveguides, or fibers, additionally, the dispersion introduced by the geometry plays a crucial role for the total dispersion. Usually, the combined effect of material anisotropy and material and geometrical dispersion must be included already at the design stage. In the previous sections, anisotropy and material dispersion were neglected. Here, their influence on our previous results for the already strongly geometrically dispersive PhC is quantified.

For FH wavelengths between 1 and 2 μm, the coherence lengths are between 3 and 16 μm utilizing d_{33} for $LiNbO_3$. This is still much shorter than for the maximum mismatch in our results presented in the previous section. Obviously, the influence of material dispersion has a similar contribution as a frequency detuning of a few percent in our case (see Fig. 3). Second, also, the material anisotropy affects the dispersion relation of the PhC Bloch modes. Because the iterative method[30] used to obtain the dispersion relation does not allow for directly accounting for material dispersion, we pursue a perturbative approach here. This is justified since in dielectrics, the changes of the dielectric tensor $\hat{\varepsilon}$ are small over a large wavelength range.

Based on the solution of the eigenvalue equation for a fixed dielectric constant in an isotropic medium, for photonic crystal fibers, a perturbative solution for the corrected frequency and group velocity was developed for the case of one isotropic dispersive component[33] or of multiple dispersive uniaxial components.[34] Because important quadratically nonlinear crystals are biaxial, we extend this approach to general anisotropic dielectric distributions of different regions of constant $\hat{\varepsilon}$ components. Because most anisotropic optical materials are only weakly anisotropic, the results can be applied to the solution for an isotropic medium to obtain the frequency for the anisotropic case.

The analysis follows Ref. 34 but allows to obtain an explicit expression for the self-consistent frequency for dispersive dielectrics, where we have a Hermitian dielectric tensor $\hat{\varepsilon}=(\varepsilon_{ij})$ instead of a scalar permittivity ε. From the vectorial wave equation in the Fourier domain,

$$\Theta\mathbf{H}=\frac{\omega^2}{c^2}\mathbf{H}, \tag{18}$$

with the linear operator $\Theta=\nabla\times[\hat{\varepsilon}^{-1}(\mathbf{r})\nabla\times\cdot]$, the eigenmodes $\mathbf{H}$ with eigenvalues ω^2/c^2 can be obtained for a fixed Bloch vector $\mathbf{k}$ and given $\hat{\varepsilon}$ using the plane wave method.[30] Conversely, we can extract the eigenvalue from a given eigenmode using the Rayleigh quotient (RQ),

$$\frac{\omega^2}{c^2}=\frac{\langle\mathbf{H},\Theta\mathbf{H}\rangle}{\langle\mathbf{H},\mathbf{H}\rangle}=:\text{RQ}. \tag{19}$$

However, if the eigenfrequency ω of the eigenmodes of a dispersive dielectric $\varepsilon_{ij}(\omega,\mathbf{r})$ is of interest, Eq. (18) must be solved in a self-consistent manner instead.

To obtain a perturbative approximation of the self-consistent frequency ω_{sc}, Eq. (18) is solved for a dielectric distribution $\hat{\varepsilon}_0(\mathbf{r})$, chosen to be close to the distribution at the expected operation frequency. This yields the frequency ω_0 and the eigenmode $\mathbf{H}(\mathbf{r})$. The structure is assumed to be piecewise constant (components $\hat{\varepsilon}^{(k)}$ with index k). Expanding about the solution $(\hat{\varepsilon}_0, \omega_0)$, we obtain for the frequency,

$$\omega_{sc} = \omega_0 + \sum_{k,i,j} \left.\frac{\partial\omega}{\partial\varepsilon_{ij}^{(k)}}\right|_{\hat{\varepsilon}=\hat{\varepsilon}_0} (\varepsilon_{ij}^{k,sc} - \varepsilon_{0,ij}^{(k)}) + \sum_k \mathcal{O}[(\hat{\varepsilon}^{k,sc} - \hat{\varepsilon}_0^{(k)})^2], \tag{20}$$

where $\hat{\varepsilon}^{k,sc} = \hat{\varepsilon}^{(k)}(\omega_{sc})$ is the corresponding self-consistent dielectric function of component k. We restrict the analysis to frequency regions, where the variation of $\hat{\varepsilon}(\omega)$, and consequently $\omega_{sc} - \omega_0$, is small and the higher order terms $\mathcal{O}[(\hat{\varepsilon}^{k,sc} - \hat{\varepsilon}_0^{(k)})^2]$ can be neglected. From Eq. (19) and the chain rule, we get

$$\frac{2\omega}{c^2}\frac{\partial\omega}{\partial\varepsilon_{ij}^{(k)}} = \frac{\partial \mathrm{RQ}}{\partial\varepsilon_{ij}^{(k)}}. \tag{21}$$

Using

$$\frac{\partial\hat{A}^{-1}}{\partial\varphi} = -\hat{A}^{-1}\frac{\partial\hat{A}}{\partial\varphi}\hat{A}^{-1}, \tag{22}$$

for the derivative of the inverse of a matrix $\hat{A}$ with respect to a parameter φ and the Hellmann-Feynman theorem,[35,36]

$$\frac{\partial \mathrm{RQ}}{\partial\varepsilon_{ij}^{(k)}} = \frac{\left\langle \mathbf{H}, \frac{\partial\Theta}{\partial\varepsilon_{ij}^{(k)}}\mathbf{H} \right\rangle}{\langle \mathbf{H}, \mathbf{H}\rangle}, \tag{23}$$

we obtain

$$\frac{\partial \mathrm{RQ}}{\partial\varepsilon_{ij}^{(k)}} = \frac{\left\langle \mathbf{H}, \nabla\times\left(\hat{\varepsilon}^{-1}\frac{\partial\hat{\varepsilon}}{\partial\varepsilon_{ij}^{(k)}}\hat{\varepsilon}^{-1}\nabla\times\mathbf{H}\right)\right\rangle}{\langle \mathbf{H}, \mathbf{H}\rangle}. \tag{24}$$

Exploiting the Hermiticity of $\nabla\times$ and $\hat{\varepsilon}$, this simplifies to

$$\frac{\partial \mathrm{RQ}}{\partial\varepsilon_{ij}^{(k)}} = -\omega^2\varepsilon_0^2\frac{\langle\hat{\varepsilon}^{(k)}\mathbf{E}, (\hat{\varepsilon}^{(k)})^{-1}(1^{ij})\mathbf{E}\rangle k}{\langle \mathbf{H}, \mathbf{H}\rangle} = -\omega^2\varepsilon_0^2\frac{\langle E_i, E_j\rangle_k}{\langle \mathbf{H}, \mathbf{H}\rangle}, \tag{25}$$

(1^{ij}) being the matrix where the coefficient $(i,j)=1$ is the only nonvanishing entry. $\langle,\rangle_k$ denotes the scalar product integrated over the component k only. Together with Eq. (21), we obtain

$$\frac{\partial\omega}{\partial\varepsilon_{ij}^{(k)}} = -\frac{\omega}{2}\frac{\langle\varepsilon_0 E_i, E_j\rangle_k}{\langle \mathbf{D}, \mathbf{E}\rangle}. \tag{26}$$

Expanding again about ω_0,

$$\varepsilon_{ij}^{k,sc} \approx \varepsilon_{ij}^{(k)}(\omega_0) + \left.\frac{\partial\varepsilon_{ij}^{(k)}}{\partial\omega}\right|_{\omega=\omega_0} (\omega_{sc} - \omega_0), \tag{27}$$

and combining this with Eqs. (20) and (25) finally yields

$$\omega_{sc} = \left[1 - \frac{\sum_{k,i,j}\frac{\langle\varepsilon_0 E_i, E_j\rangle_k}{\langle \mathbf{D}, \mathbf{E}\rangle}(\varepsilon_{ij}^{(k)}(\omega_0) - \omega_{0,ij}^{(k)})}{2 + \omega_0\sum_{k,i,j}\frac{\langle\varepsilon_0 E_i, E_j\rangle_k}{\langle \mathbf{D}, \mathbf{E}\rangle}\left.\frac{\partial\varepsilon_{ij}^{(k)}}{\partial\omega}\right|_{\omega=\omega_0}}\right]\omega_0, \tag{28}$$

as the approximate solution for the self-consistent frequency in a structure with a nonabsorbing, piecewise homogeneous, slightly dispersive dielectric function. Because nondegenerate perturbation theory was used to obtain this result, it only applies to well-separated (nondegenerate) bands. Otherwise, the unperturbed solutions have to be chosen such that the perturbation is diagonal in this subspace.

We apply this method to the band structure obtained for isotropic $LiNbO_3$. The values for the frequency and temperature dependent ordinary and extraordinary indices are taken from Ref. 29, for a temperature of 293.15 K. The lattice constant was $a=600$ nm. Both calculations lead to the same final band structure, where obviously the 60° symmetry is lifted. For our orientation of the crystal's Z axis along x in the laboratory frame, we find a new frequency of perfect phase match (see Fig. 3) $u_f=0.264\,18$ corresponding to a wavelength of $\lambda_f=2.271$ μm, compared to the wavelength $\lambda_f=2.116$ μm obtained from the renormalization of the values without anisotropy and material dispersion. In order to compensate for this wavelength shift of more than 150 nm, there are two adjustable parameters: first, the temperature, and second, the hole size. A hole size of $r/a=0.325$ turned out to give phase match at the original frequency, as can be seen from the back-shifted mismatch curve in Fig. 3.

To sum up, if material dispersion and anisotropy should be included at the design stage of such a PhC based device, at the fabrication stage, the desired hole size has to be met with a tolerance of a few nanometers.

VI. CONCLUSIONS

We investigated theoretically slow-light enhanced wide-beam degenerate SHG in a 2D PhC. The PhC provides the noncritical collinear phase matching of the FH and SH waves with simultaneously low group velocities. A total enhancement of the SHG efficiency of a factor of 60 compared to a QPM homogeneous medium is verified, which is obtained for a hole radius of 189 nm. For other propagation directions, noncritically phase matched backward SHG is possible. The influence of material dispersion and anisotropy is discussed for lithium niobate.

Based on the reciprocity theorem with a quadratic nonlinear perturbative polarization, we derived equations for the slowly varying envelopes of the linear modal fields (normal modes) which are the Bloch modes of the photonic crystal. This is compared to results obtained by means of a nonlinear version of the FDTD method. Here, the propagation of TE polarized light in a hexagonal PhC in $LiNbO_3$ is modeled without further approximation, and excellent agreement with the modal approach is found. The conversion efficiency and phase mismatch could be properly predicted from the linear modal field overlaps and the dispersion relation. For instance, for a hole radius of 180 nm, the propagation length

scales with a factor of 1.5 compared to a homogeneous medium, although the structure has a 32.6% air filling fraction. The factor of 1.3 obtained from the field overlaps of the modal approach is in good agreement, given the fact that a number of higher order integrals have to be computed accurately from numerical data. The origin of this larger efficiency is the slow group velocity of the FH and SH waves, originating from multiple scattering of the light traveling along the ΓM direction in the periodic medium. This corresponds to an effectively increased path length. However, due to the very different scattering behavior at the two frequencies, the overlap is decreased compared to a homogeneous medium.

To calculate the dispersion relation taking into account material dispersion and anisotropy, a perturbative method was extended and used in conjunction with the plane wave method. The associated shift of the previously phase matched Bloch modes leads to the original frequency being in the modal gap. To compensate for this, the hole radius has to be increased by 8%.

ACKNOWLEDGMENTS

R.I. gratefully acknowledges a grant by the Carl Zeiss Foundation. In addition, financial support by the Federal Ministry of Education and Research (Innoregio, ZIK) is acknowledged.

*rumen.iliew@uni-jena.de

[1] P. A. Franken, A. E. Hill, C. W. Peters, and G. Weinreich, Phys. Rev. Lett. **7**, 118 (1961).
[2] J. A. Armstrong, N. Bloembergen, J. Ducuing, and P. S. Pershan, Phys. Rev. **127**, 1918 (1962).
[3] G. D. Boyd and D. A. Kleinman, J. Appl. Phys. **39**, 3597 (1968).
[4] D. S. Hum and M. M. Fejer, C. R. Phys. **8**, 180 (2007), and references therein.
[5] V. Berger, Phys. Rev. Lett. **81**, 4136 (1998).
[6] N. G. R. Broderick, G. W. Ross, H. L. Offerhaus, D. J. Richardson, and D. C. Hanna, Phys. Rev. Lett. **84**, 4345 (2000).
[7] N. Bloembergen and A. J. Sievers, Appl. Phys. Lett. **17**, 483 (1970).
[8] A. Yariv and P. Yeh, J. Opt. Soc. Am. **67**, 438 (1977).
[9] C. L. Tang and P. P. Bey, IEEE J. Quantum Electron. **9**, 9 (1973).
[10] J. P. van der Ziel and M. Ilegems, Appl. Phys. Lett. **28**, 437 (1976).
[11] J. Martorell and R. Corbalán, Opt. Commun. **108**, 319 (1994).
[12] M. Scalora, M. J. Bloemer, A. S. Manka, J. P. Dowling, C. M. Bowden, R. Viswanathan, and J. W. Haus, Phys. Rev. A **56**, 3166 (1997).
[13] M. Bertolotti, J. Opt. A, Pure Appl. Opt. **8**, S9 (2006), and references therein.
[14] K. Sakoda and K. Ohtaka, Phys. Rev. B **54**, 5742 (1996).
[15] A. Di Falco, C. Conti, and G. Assanto, Opt. Lett. **30**, 1174 (2005).
[16] A. Di Falco, C. Conti, and G. Assanto, Opt. Lett. **31**, 250 (2006).
[17] R. Iliew, C. Etrich, U. Peschel, and F. Lederer, IEEE J. Sel. Top. Quantum Electron. **12**, 377 (2006).
[18] R. Iliew, C. Etrich, M. Augustin, E.-B. Kley, S. Nolte, A. Tünnermann, and F. Lederer, Phys. Status Solidi A **204**, 3689 (2007).
[19] E. Centeno, D. Felbacq, and D. Cassagne, Phys. Rev. Lett. **98**, 263903 (2007).
[20] K. Staliunas, Y. Loiko, R. Herrero, C. Cojocaru, and J. Trull, Opt. Lett. **32**, 1992 (2007).
[21] F. Schrempel, T. Gischkat, H. Hartung, E.-B. Kley, and W. Wesch, Nucl. Instrum. Methods Phys. Res. B **250**, 164 (2006).
[22] M.-P. Bernal, N. Courjal, J. Amet, M. Roussey, and C. Hou, Opt. Commun. **265**, 180 (2006).
[23] A. Taflove and S. C. Hagness, *Computational Electrodynamics: The Finite-Difference Time-Domain Method* (Artech House, Boston, MA, 2000).
[24] L. Tkeshelashvili and K. Busch, Appl. Phys. B: Lasers Opt. **81**, 225 (2005).
[25] A. W. Snyder and J. D. Love, *Optical Waveguide Theory* (Chapman and Hall, London, 1983).
[26] D. Michaelis, U. Peschel, C. Wächter, and A. Bräuer, Phys. Rev. E **68**, 065601(R) (2003).
[27] P. Yeh, J. Opt. Soc. Am. **69**, 742 (1979).
[28] Y. Xu, R. K. Lee, and A. Yariv, J. Opt. Soc. Am. B **17**, 387 (2000).
[29] M. V. Hobden and J. Warner, Phys. Lett. **22**, 243 (1966).
[30] S. G. Johnson and J. D. Joannopoulos, Opt. Express **8**, 173 (2001).
[31] C. M. Reinke, A. Jafarpour, B. Momeni, M. Soltani, S. Khorasani, A. Adibi, Y. Xu, and R. K. Lee, J. Lightwave Technol. **24**, 624 (2006).
[32] M. Lauritano, M. Girotto, G. Bellanca, and S. Trillo, Opt. Quantum Electron. **38**, 827 (2006).
[33] J. Lægsgaard, A. Bjarklev, and S. E. Barkou Libori, J. Opt. Soc. Am. B **20**, 443 (2003).
[34] P. D. Rasmussen, J. Lægsgaard, and O. Bang, J. Opt. Soc. Am. B **23**, 2241 (2006).
[35] H. Hellmann, Z. Phys. **85**, 180 (1933).
[36] R. P. Feynman, Phys. Rev. **56**, 340 (1939).